

## RESEARCH ARTICLE

# Ethylenediaminetetraacetate functionalized MgFe layered double hydroxide/biochar composites for highly efficient adsorptive removal of lead ions from aqueous solutions

M. T. Amin<sup>1,2\*</sup>, A. A. Alazba<sup>1,3</sup>, M. Shafiq<sup>1</sup>

**1** Alamoudi Water Research Chair, King Saud University, Riyadh, Kingdom of Saudi Arabia, **2** Department of Environmental Sciences, COMSATS University Islamabad, Abbottabad, Pakistan, **3** Agricultural Engineering Department, King Saud University, Riyadh, Kingdom of Saudi Arabia

\* [mtamin@ksu.edu.sa](mailto:mtamin@ksu.edu.sa)

## OPEN ACCESS

**Citation:** Amin MT, Alazba AA, Shafiq M (2022) Ethylenediaminetetraacetate functionalized MgFe layered double hydroxide/biochar composites for highly efficient adsorptive removal of lead ions from aqueous solutions. PLoS ONE 17(3): e0265024. <https://doi.org/10.1371/journal.pone.0265024>

**Editor:** Amit Bhatnagar, Lappeenranta-Lahti University of Technology (LUT University), FINLAND

**Received:** November 22, 2021

**Accepted:** February 20, 2022

**Published:** March 3, 2022

**Copyright:** © 2022 Amin et al. This is an open access article distributed under the terms of the [Creative Commons Attribution License](https://creativecommons.org/licenses/by/4.0/), which permits unrestricted use, distribution, and reproduction in any medium, provided the original author and source are credited.

**Data Availability Statement:** All relevant data are within the manuscript.

**Funding:** This project was funded by the National Plan for Science, Technology and Innovation (MAARIFAH), King Abdulaziz City for Science and Technology, Kingdom of Saudi Arabia, Award Number (12-WAT2623-02) The funders had no role in study design, data collection and analysis,

## Abstract

The application of layered double hydroxides (LDHs) of MgFe and its composites with biochar of *Eucalyptus camdulensis* (Eb) and ethylenediaminetetraacetic acid (EDTA) was explored in a batch study to mitigate toxic lead ions ( $Pb^{2+}$ ) from synthetic wastewater solutions. SEM images revealed that MgFe/LDH composites with Eb were successfully formed, while FTIR spectra confirmed the successful adsorption of  $Pb^{2+}$  onto the MgFe/LDH and composite adsorbents. Batch equilibrium was attained after 60 min, then the adsorption capacity gradually increased. An increase in adsorption capacity (and a 60% decrease in the percentage removal) was observed by increasing the initial  $Pb^{2+}$  concentration, and the highest value was  $136\text{ mg g}^{-1}$  for MgFe/LDH-Eb\_EDTA. A 50–60% increase in both the adsorption capacities and percent removal was seen in the pH range of 2–6. The second-order kinetic model had a nearly perfect fitting, suggesting that chemisorption was the mechanism controlling adsorption. The Langmuir isotherm model best presented the adsorption data, suggesting that the  $Pb^{2+}$  adsorption was monolayer, and predicted a better affinity between the adsorbent surface and adsorbed  $Pb^{2+}$  for MgFe/LDH-Eb\_EDTA in comparison to the other two adsorbents. The D–R isotherm suggested that the adsorption system was physical based on  $E$  values for all three adsorbents, while the Temkin isotherm model suggested that  $Pb^{2+}$  adsorption was heterogeneous. Finally, the Sips and R–P isotherms predicted that the adsorption of  $Pb^{2+}$  on the surface of the adsorbents was homogeneous and heterogeneous.

## 1. Introduction

The increase in heavy metal toxicity in natural freshwater reservoirs due to industrial growth has recently attracted much attention [1,2]. Lead (Pb), copper (Cu), arsenic (As), and cadmium (Cd) are very dangerous and highly toxic heavy metals that are typically found in

decision to publish, or preparation of the manuscript.

**Competing interests:** The authors have declared that no competing interests exist.

industrial wastewater due to their tendency to bioaccumulate through the food chain; as a result, they cause harmful effects on livestock, aquatic life and human health [3–5]. Lead ions ( $Pb^{2+}$ ) are among the most common heavy metal ions with carcinogenic features and are often present in tannery, electroplating, metallurgical processes, pesticides, chemical processing, matching, photographic film, battery recycling processes, explosives, paint and pigment, and refinery wastewater [6]. Exposure to  $Pb^{2+}$  may result in severe poisoning in the liver and kidneys, as well as problems in blood pressure, mental retardation in children, reproductive system damage, and central nervous system damage [7,8]. Therefore, the unregulated disposal of effluents into fresh water supplies without treatment may cause shortages of fresh drinking water that is safe and clean. It has already been reported that approximately 25 million deaths worldwide are caused by the consumption of polluted drinking water [9]. Governments/policy-makers should, therefore, impose strict regulations on the management of industrial effluents to safeguard humanity from this serious danger. Therefore, researchers and scientists should come forward and help industries establish cheap, efficient, and eco-friendly methods for removing aqueous  $Pb^{2+}$  or other contaminants from industrial wastewater before being discharged into land and natural aquatic systems.

Many techniques, including chemical precipitation, ion exchange, electrocoagulation, reverse osmosis, solvent extraction and adsorption, have been established by different scientists for wastewater treatment [10]. Nevertheless, compared to conventional wastewater treatment technologies, adsorption is considered to be a very effective method due to its low cost, simplicity in implementation/operation, separation efficiency, and higher potential to adsorb heavy metals from low to higher concentrations [11–13]. Hence, choosing the most suitable and effective adsorbent with the highest stability, selectivity, and efficiency is very important. Various types of low-cost and efficient adsorbents, such as activated carbon, biochar, silica, zeolite, industrial byproducts, agricultural wastes, polymeric materials and clay minerals, and composite materials have been developed and studied conventionally to extract inorganic and organic contaminants from industrial wastewater [14–21]. However, this area of research has not yet been fully explored and needs further study. Therefore, there is an ongoing initiative to produce a high-quality and affordable adsorbent material that can be easily separated after being adsorbed from aqueous solution to prevent secondary contamination [22].

Layered double hydroxides (LDHs) have recently been found to be very efficient adsorbents because of their high surface area, low cost, large interlayer spaces (porosity), heat resistant structure, and large number of exchangeable anions with high anionic exchange capacities, making them excellent and desirable materials for use in adsorption [23,24]. The general formula of LDH is  $[M^{2+}_{1-x}M^{3+}_x(OH)_2]A^{n-}_{x/n}yH_2O$ , where  $M^{2+}$  and  $M^{3+}$  are divalent and trivalent metal ions, respectively.  $A^{n-}$  represents an anion, and  $x$  is the ratio of  $M^{3+}/(M^{2+} + M^{3+})$  [25]. The main property of LDH is that the anion present in the interlayer can be easily exchanged by the other anions so that LDHs can be used to extract a number of inorganic anions, such as phosphate, arsenate, bromate and fluoride, from aqueous solution [26–28]. Studies are being performed to increase the efficiency of LDH materials by intercalating LDH with chelating agents such as maltase, glutamate, and citrate, and an excellent heavy metal extraction from wastewater was achieved due to the formation of chelating complexes [29]. Some ongoing studies are also developing a combination of LDH with porous and functional materials such as agricultural or industrial porous carbon (biochar, activated carbon) that is waste-based, as well as graphene or graphite [30]. Hence, the present study aimed to obtain more active adsorption sites on the surface of LDH by mixing it with *Eucalyptus camdulensis* (*Ec*) tree bark waste, which can be used as a source of porous green carbon, and ethylenediaminetetraacetic acid (EDTA), which is a very popular and powerful chelating material with abundant functional groups (amino and carboxyl). It was hypothesized that the addition of *Ec*

(Eb) biochar and EDTA with LDH can possibly generate a stable and highly efficient adsorbent that can effectively remove lead ions from wastewater.

The aim of this work was to develop and characterize LDHs of MgFe and its composites with Eb (MgFe/LDH-Eb) and with Eb and EDTA (MgFe/LDH-Eb\_EDTA) and to study their potential capacity to remove toxic  $Pb^{2+}$  from synthetic wastewater solutions based on the stability of chelates formed between EDTA and  $Pb^{2+}$ . The endeavor of comparing the performance of the simple and composite adsorbents, that has not been performed previously, is the focus of this work so that an efficient treatment system can be developed for aqueous systems. Additionally, the effects of pH, contact time, and initial concentration of  $Pb^{2+}$  and the amount of adsorbent on the adsorption of  $Pb^{2+}$  onto the synthesized adsorbents were examined. Isotherm and kinetic models were applied to the adsorption data to gain knowledge on the  $Pb^{2+}$  removal process.

## 2. Materials and methods

### 2.1. Chemical and adsorbent preparations

All the chemicals used in this study were of analytical reagent grade, including the lead nitrate that was used to prepare the stock solution ( $1000 \text{ mg L}^{-1}$ ) of the model contaminant by dissolving 1.0 g of it ( $Pb(NO_3)_2$ , Tianjin Benchmark Chemical Reagent Co., Ltd. Tianjin, China) in 1.0 liter of deionized water. The prepared stock solution was further diluted to prepare working solutions with different initial concentrations of  $Pb^{2+}$  using deionized water. To maintain and adjust the solution pH as necessary for each batch test, 0.1 M NaOH and 0.1 M  $HNO_3$  were used.

Eb was prepared as reported previously [31], using *Ec* waste obtained from local areas around the city of Riyadh, Kingdom of Saudi Arabia. The collected waste was washed rigorously and thoroughly dried in an open atmosphere, and then the oven-dried (at  $80^\circ\text{C}$  for 6 hours) product was crushed in a ball mill to obtain an average particle size of nearly 5.0 mm. Finally, a box furnace (Nabertherm, B-150, Germany) was operated for 3 h at  $600^\circ\text{C}$  for the pyrolysis process to achieve biochar with an average particle size of 50–70  $\mu\text{m}$ .

Magnesium nitrate hexahydrate ( $Mg(NO_3)_2 \cdot 6H_2O$ ) and iron(III) nitrate nonhydrate ( $Fe(NO_3)_3 \cdot 9H_2O$ ) were used to prepare the LDH of MgFe with a  $Fe^{2+}/Mg^{3+}$  ratio of 1:2. A simple coprecipitation method was adopted in which both solutions were agitated in deionized water by maintaining the solution pH at 10.0, and ammonia was added dropwise with vigorous stirring to form the precipitate in approximately 30 min.

Composites from the prepared LDH of MgFe with Eb and Eb\_EDTA were prepared by adding 3 and 5 g of Eb and EDTA, respectively, to 4 and 5 g (20% and 25%) of  $Mg(NO_3)_2 \cdot 6H_2O$  and  $Fe(NO_3)_3 \cdot 9H_2O$  solutions, respectively. The slurry was filtered and washed several times using double distilled water until the neutral pH became neutral. The resultant solutions were finally dried at  $60^\circ\text{C}$  for 24 h in an ordinary oven.

### 2.2. Methodology and batch testing

**2.2.1. Characterization.** Scanning electron microscopy (SEM), energy dispersive X-ray (EDX) technique and Fourier transform infrared (FTIR) spectrometry were used to investigate the morphology and to obtain insight into the chemical composition of the MgFe/LDH and composite adsorbents before and after the heavy metal ions being studied were adsorbed. A quick comparison among the LDH, Eb and composite adsorbents (MgFe/LDH-Eb and MgFe/LDH-Eb\_EDTA) was performed based on the pore structure and specific surface area measurement using Brunauer–Emmett–Teller (BET) analysis.

**2.2.2. Adsorption experiments.** To obtain the necessary amount of each adsorbent in different batch tests, appropriate amounts of MgFe/LDH and its composites were measured based on the volume of the tested solution and initial  $\text{Pb}^{2+}$  concentrations. For the batch experiments, 50 or 100 mL of the suspensions were placed inside conical flasks and agitated at 220 rpm using a temperature-controlled (30°C) shaker (Wise Cube orbital, Wisd. ThermoStable IS-20; Daihan Scientific Co. Ltd., South Korea). After being agitated for a predetermined contact time, 5 mL of the sample was filtered through 0.45  $\mu\text{m}$  (Whatman™) filters and inserted into a flame atomic absorption spectrometer (FAAS, Thermo Scientific, ICE 3000 Series, Cambridge, United Kingdom) to measure the residual metal concentration ( $C_t$ ,  $\text{mg L}^{-1}$ ). The adsorption capacity ( $q_b$ ,  $\text{mg g}^{-1}$ ) of the adsorbent and the percentage of  $\text{Pb}^{2+}$  removal was obtained using the initial ( $C_0$ ,  $\text{mg L}^{-1}$ ) and residual metal concentrations using Eqs (1) and (2), respectively.  $V$  (L) and  $m$  (g) represent the volume of the solution and the weight of the adsorbent, respectively.

$$\text{Adsorption capacity} = \left( \frac{C_0 - C_t}{m} \right) V \quad (1)$$

$$\text{Removal (\%)} = \left( \frac{C_0 - C_t}{C_0} \right) \times 100 \quad (2)$$

Batch tests for optimization of parameters (contact time, solution pH, amount of adsorbent and initial  $\text{Pb}^{2+}$  concentration) were conducted by taking samples at least thrice while their average values are presented in Figs 3 and 4. The one-way analysis of variance was performed with the least significant difference of means at  $p = 0.01$ . Additional samples were taken whenever the difference between two measurements exceeded by 5%. The measurement of the equilibrium contact time was carried out at different initial concentrations (20–50  $\text{mg L}^{-1}$ ) of  $\text{Pb}^{2+}$ . For this purpose, the amount of the adsorbent was fixed at 0.3 g, while the solution pH was maintained at 6.0 over a contact time range of 1–300 min. The optimum initial  $\text{Pb}^{2+}$  concentration was determined by performing batch tests in the range of 20–100  $\text{mg L}^{-1}$ . The analysis was carried out at an optimized contact time of 60 min with a fixed amount of the adsorbent and solution pH of 0.3 g and 6.0, respectively. Batch tests for optimizing the solution pH were conducted in the range of 2–9, as shown in Fig 4B. For this purpose, 0.3 g of the adsorbent was added to the solution with an initial  $\text{Pb}^{2+}$  concentration of 40  $\text{mg L}^{-1}$ , and the samples were withdrawn after 60 min of contact time. Among the other important batch parameters, the amount of the adsorbent was also optimized due to its direct effects on the cost of the adsorption process. The adsorption performance was tested with the amount of adsorbent in ranges of 0.05–0.5 g by fixing the solution pH and initial  $\text{Pb}^{2+}$  concentration at 6.0 and 40  $\text{mg L}^{-1}$ , respectively, while suspensions were agitated for 60 min of contact time. Finally, the desorption experiments at different initial solution pH and temperatures were performed by using 0.1 M hydrochloric acid as an eluent in addition to a mild heat treatment inside an oven for 24h.

## 3. Results and discussions

### 3.1. Characteristics of the adsorbents

**3.1.1. Scanning electron microscopy analysis.** The intercalation performance and surface structure of MgFe/LDH, its composite with the biochar of *Ec* (MgFe/LDH-Eb) and EDTA-functionalized composite adsorbent (MgFe/LDH-Eb\_EDTA) before and after adsorption of  $\text{Pb}^{2+}$  ions were investigated by SEM observations, as depicted in Fig 1. The images of MgFe/LDH before and after  $\text{Pb}^{2+}$  adsorption are displayed in Fig 1A & 1D. Clumping of flowers,

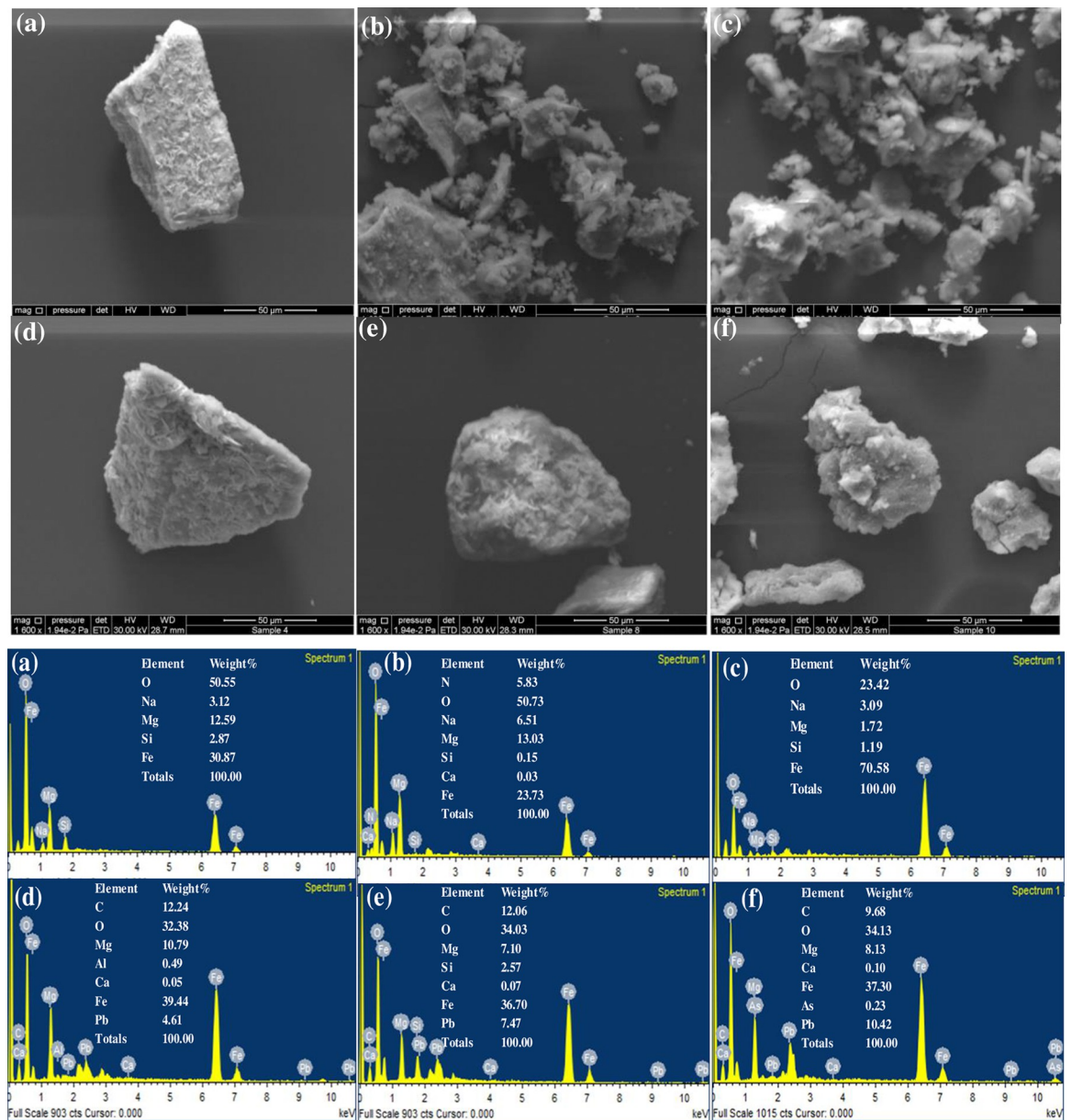


**Fig 1.** a. SEM images before and after adsorption of Pb<sup>2+</sup>; MgFe/LDH (a, d), MgFe/LDH-Eb (b, e) and MgFe/LDH-Eb\_EDTA (c, f). b. EDX spectra before and after adsorption of Pb<sup>2+</sup>; MgFe/LDH (a, d), MgFe/LDH-Eb (b, e) and MgFe/LDH-Eb\_EDTA (c, f).

<https://doi.org/10.1371/journal.pone.0265024.g001>

such as MgFe/LDH ultrafine nano glitter microspheres that were entangled with each other, can be clearly seen in the images [32,33]. Fig 1B & 1E shows SEM images of the MgFe/LDH-Eb composite before and after adsorption of Pb<sup>2+</sup>. The porous and rough surface of biochar particles in addition to MgFe/LDH on the surface of biochar depicted successful formation of the MgFe/LDH composite with the biochar of *Ec*. Fig 1C & 1F shows that the SEM images of EDTA treated with the biochar of *Ec* and MgFe/LDH composites before and after adsorption of Pb<sup>2+</sup> were shiny and porous and had aggregates with irregular structures [34].

Furthermore, to confirm the mechanism and elemental composition of MgFe/LDH and composite adsorbents, EDX spectra of pre and post adsorption of Pb<sup>2+</sup> are shown in Fig 1B.

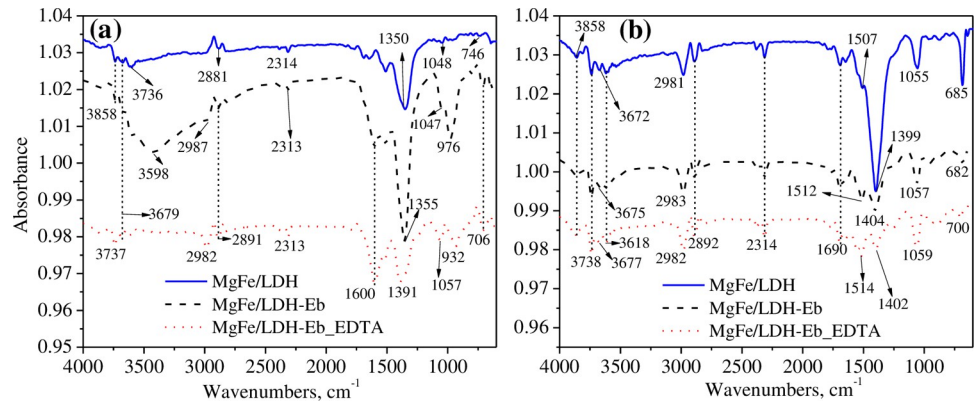


**Fig 2.** FTIR spectra of MgFe/LDH and composite adsorbents before (a) and after (b) adsorption of  $Pb^{2+}$ .

<https://doi.org/10.1371/journal.pone.0265024.g002>

The elemental content in pre adsorption (Fig 1B (a, b, c)) samples changed immediately after  $Pb^{2+}$  adsorption, as can be clearly seen in Fig 1B (d, e, f) spectra of post adsorption samples. The change in elemental content during  $Pb^{2+}$  adsorption indicates that ion exchange on the surface and in the interlayer of the synthesized adsorbent material was involved [35].

**3.1.2. Fourier transform infrared analysis.** The type of functional groups and the change in chemical bonding perceived on the surface of MgFe/LDH and composite adsorbents before and after the adsorption of  $Pb^{2+}$  were investigated using the FTIR technique, as shown in Fig 2. Noticeably, the spectra of all three adsorbents before adsorption showed distinct FTIR bands for the biochar, MgFe/LDH, and EDTA, as presented in Fig 2A. When MgFe/LDH was composited with the biochar of *Ec* and then functionalized with EDTA, a small peak appeared at approximately  $3736\text{ cm}^{-1}$ , and this peak moved to  $3737\text{ cm}^{-1}$  and can be denoted as inter-layer water and hydroxyl group stretching vibrations. According to the literature, LDH adsorption peaks below  $3800\text{ cm}^{-1}$  to  $3200\text{ cm}^{-1}$  often represent OH hydroxyl groups that are associated with the presence of  $H_2O$  (interlayer water molecules) [33,36]. The characteristic peaks at approximately  $2987$  and  $2881\text{ cm}^{-1}$  were shifted to  $2982$  and  $2891\text{ cm}^{-1}$ , and these were attributed to C-H groups [37]. Low intensity peaks appeared at frequencies of approximately  $2314\text{ cm}^{-1}$  in MgFe/LDH and  $2313\text{ cm}^{-1}$  in the MgFe/LDH-Eb and MgFe/LDH-Eb\_EDTA spectra, which correspond to the C-O band related to  $CO_2$  [37]. Another large peak observed at a frequency of  $1600\text{ cm}^{-1}$  in the spectra of MgFe/LDH-Eb and MgFe/LDH-Eb\_EDTA is due to the O-H bending vibration from the adsorbed water molecules [36].

Other prominent peaks were observed at a frequency of  $1350\text{ cm}^{-1}$  in the MgFe/LDH spectra, while peaks at  $1355\text{ cm}^{-1}$  in the MgFe/LDH-Eb spectra and  $1391\text{ cm}^{-1}$  in MgFe/LDH-Eb\_EDTA corresponded to stretching vibration modes of N-O [36,38,39]. Additionally, the N-O stretching band can clearly be identified in the regions of  $1500\text{--}1200\text{ cm}^{-1}$  and  $1080\text{--}1020\text{ cm}^{-1}$  [39]. The very sharp peaks observed at  $976\text{ cm}^{-1}$  in the MgFe/LDH-Eb spectra and at  $932$  and  $706\text{ cm}^{-1}$  in MgFe/LDH-Eb\_EDTA were attributed to M-O-H or O-M-O groups [40]. The MgFe/LDH spectra and composite adsorbents spectra after  $Pb^{2+}$  adsorption are shown in Fig 2B. Most of the absorption bands remained unchanged, or very little change in frequencies was observed. Therefore, only new absorption bands appearing after  $Pb^{2+}$  adsorption will be discussed here. A very prominent band shift was observed from  $1600\text{ cm}^{-1}$  to  $1690\text{ cm}^{-1}$  in all three adsorbents, and this band was ascribed to the bending vibration of water molecules [41]. New bands appearing at  $1507\text{ cm}^{-1}$  (MgFe/LDH loaded  $Pb^{2+}$ ),  $1512\text{ cm}^{-1}$  (MgFe/LDH-Eb loaded  $Pb^{2+}$ ) and  $1514\text{ cm}^{-1}$  in (MgFe/LDH-Eb\_EDTA loaded  $Pb^{2+}$ ) were ascribed to N-O stretching [39]. Another major band shift was observed at  $1399\text{ cm}^{-1}$  in the MgFe/LDH-loaded

Pb<sup>2+</sup> spectra, 1404 cm<sup>-1</sup> in MgFe/LDH-Eb-loaded Pb<sup>2+</sup> and 1402 cm<sup>-1</sup> in MgFe/LDH-Eb\_EDTA-loaded Pb<sup>2+</sup>, which was ascribed to the N-O bending vibration of NO<sub>3</sub><sup>-</sup> ions. Likewise, the bands at 685, 682 and 700 cm<sup>-1</sup> were ascribed to metal oxygen or hydroxyl oxygen bands (Pb-O, Pb-OH or O-Pb-O), suggesting that Pb<sup>2+</sup> had adsorbed onto the tested adsorbents. Thus, these results indicated that Pb<sup>2+</sup> was successfully adsorbed onto the MgFe/LDH and composite adsorbents.

### 3.2. Effects of the batch parameters on the adsorption process

Fig 3 presents the changes in the removal efficiency and adsorption capacity of MgFe/LDH as well as the composite adsorbents at an initial concentration of 20 mg L<sup>-1</sup> Pb<sup>2+</sup>. A very high removal of Pb<sup>2+</sup> was evident upon immediate contact (more than 50% after only 1.0 min) due to the abundance of free active sites on the surface of the adsorbent. The removal rate continued to be high for up to 5 min of contact time with a greater than 90% removal efficiency for MgFe/LDH-Eb\_EDTA at low initial concentrations of Pb<sup>2+</sup> (20 and 30 mg L<sup>-1</sup>). A gradual increase in the adsorption capacity and removal efficiency was observed when the equilibrium contact time at 60 min was attained, as shown in Fig 3. No further increase in the adsorption capacity or removal efficiency was seen for any adsorbent at any initial Pb<sup>2+</sup> concentration. At 60 min, the maximum adsorption capacity and removal efficiency of 63 mg g<sup>-1</sup> and 97%, respectively, were seen for MgFe/LDH-Eb\_EDTA, while these were nearly 55 mg g<sup>-1</sup> and 86% (maximum adsorption capacity and removal efficiency) for both MgFe/LDH and MgFe/LDH-Eb, respectively, owing to the higher surface area of MgFe/LDH-Eb\_EDTA compared to that of the other two adsorbents. As per multi-point BET and Barrett–Joyner–Halenda measurements, specific area of MgFe/LDH was estimated nearly 114 m<sup>2</sup> g<sup>-1</sup> with a pore volume and diameter of 0.37 cm<sup>3</sup> g<sup>-1</sup> and 3.4 nm, respectively. A high BET specific surface areas of about 127.5 and 141 m<sup>2</sup> g<sup>-1</sup> were measured, respectively, for MgFe/LDH-Eb and MgFe/LDH-Eb\_EDTA.

An increase in adsorption capacity by increasing the initial Pb<sup>2+</sup> concentration was observed for all three adsorbents with a maximum adsorption capacity at 60 mg L<sup>-1</sup> due to the existence of a stronger driving force between the surface of the adsorbent and high Pb<sup>2+</sup> in concentrated solution [42,43]. These values were recorded as 136, 119, and 116 mg g<sup>-1</sup> for MgFe/LDH-Eb\_EDTA, MgFe/LDH-Eb and MgFe/LDH, respectively, as shown in Fig 4A.

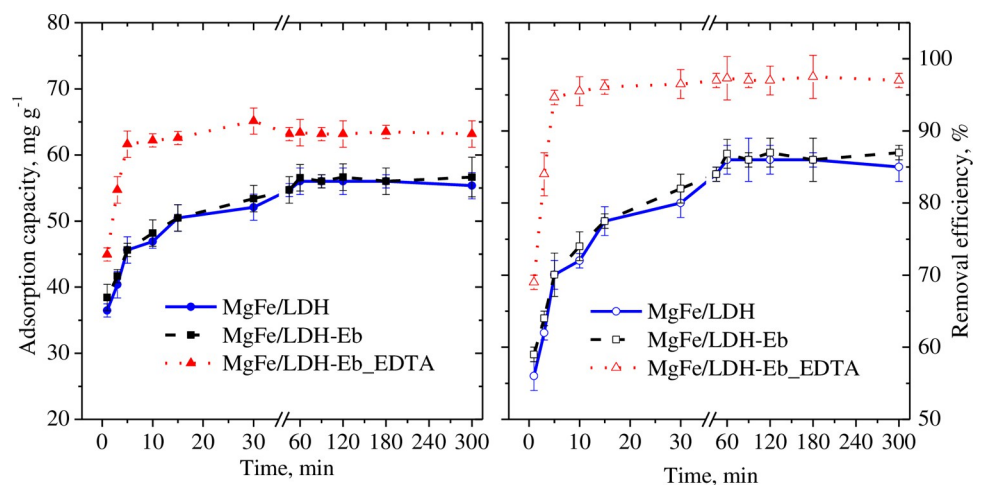
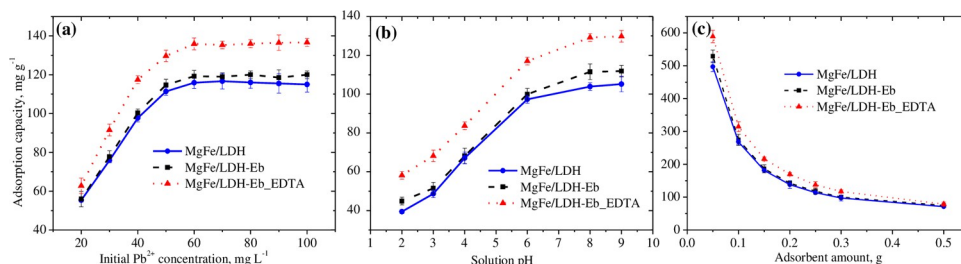


Fig 3. Effect of the contact time on the adsorption capacities and removal efficiencies of Pb<sup>2+</sup> (20 mg L<sup>-1</sup>) by MgFe/LDH, MgFe/LDH-Eb, and MgFe/LDH-Eb\_EDTA.

<https://doi.org/10.1371/journal.pone.0265024.g003>



**Fig 4.** Effects of the initial Pb<sup>2+</sup> concentration (a), solution pH (b), and adsorbent amount on the adsorption capacities and removal efficiencies of Pb<sup>2+</sup> by MgFe/LDH, MgFe/LDH-Eb, and MgFe/LDH-Eb\_EDTA.

<https://doi.org/10.1371/journal.pone.0265024.g004>

Nearly insignificant changes ( $p = 0.01$ ) in adsorption capacities were seen in the initial Pb<sup>2+</sup> concentration range of 60–100 mg L<sup>-1</sup>. On the other hand, a nearly 60% decrease in the percentage of Pb<sup>2+</sup> removal by all three adsorbents in the selected range of initial Pb<sup>2+</sup> concentrations (20–100 mg L<sup>-1</sup>) is associated with the decreasing active sites of a fixed adsorbent (0.3 g) amount for high Pb<sup>2+</sup> concentrations. In other words, the saturation of the active sites on the surface of adsorbents occurs due to its fixed amount (0.3 g) and thus these active sites become unavailable for increased initial concentrations of Pb<sup>2+</sup>, as previously reported for different adsorption systems [44–47].

Similar trends for changes in the adsorption capacities and percentage removal were seen for all three adsorbents, wherein a significant increase in both parameters was observed as the solution pH increased from 2.0 to 6.0. In acidic conditions with solution pH 2.0 to 4.0, the low efficiency of the adsorption is resulted due to the competition between the divalent Pb<sup>2+</sup> and an excess amount of H<sup>+</sup> ions to attach to the negatively charged surface of the adsorbent [48,49]. Nearly 50–60% increases in the adsorption capacities and percentage removal were seen in the aforementioned range of pH values. Insignificant changes were observed in the adsorption performance as the pH increased from 6.0 to 8.0, whereas both the adsorption capacities and percentage of removal remained almost constant beyond a solution pH of 8.0. The maximum adsorption capacity at a solution pH of 8.0 was found to be 130 mg g<sup>-1</sup> for MgFe/LDH-Eb\_EDTA, with corresponding values of 112 and 104 mg g<sup>-1</sup> for MgFe/LDH-Eb and MgFe/LDH, respectively. A reduction in the amount of H<sup>+</sup> with increasing solution pH causes the divalent Pb<sup>2+</sup> to attach to the surface of the adsorbent with less competition, resulting in increased adsorption capacity and percentage of removal [48–50].

A nearly similar trend of decreasing adsorption capacities and increasing removal efficiency was assessed for all three adsorbents by increasing the corresponding amount of adsorbents, as shown in Fig 4C. A maximum adsorption capacity of 589 mg g<sup>-1</sup> corresponded to a percentage removal of 75% at the lowest tested amount of the composite adsorbent, MgFe/LDH-Eb\_EDTA, i.e., which was 0.05 g. The corresponding maximum adsorption capacities at the same adsorbent amount (0.05 g) were recorded as 529 and 497 mg g<sup>-1</sup> for MgFe/LDH-Eb and MgFe/LDH, respectively. A decreasing trend in adsorption capacities with an increased amount of the adsorbent was attributed to the availability of more free active sites for a fixed Pb<sup>2+</sup> concentration (40 mg L<sup>-1</sup>). Although, the large surface area of the increasing amount of adsorbent is good for the efficiency of the adsorption process but the amount of the adsorbent has a direct effect on the adsorption system in terms of its cost-effectiveness, so it is always important to know the optimum value.

Considering the importance of regeneration for practical applications, the adsorption capacity of the composite adsorbent was estimated for Pb<sup>2+</sup> and it was found that the amount of desorbed Pb<sup>2+</sup> decreased by increasing the temperature. Moreover, a high amount of Pb<sup>2+</sup>

was desorbed with average desorption rate of nearly 100% at low solution pH (2.0–4.5). Finally, Table 1 provides a quick comparison for the obtained maximum adsorption capacities of the investigated adsorbents in this study with other similar adsorbents, as reported in the literature.

### 3.3. Modeling of the experimental data using adsorption kinetics

The nonlinear expressions of the most commonly used kinetic models are expressed using Eqs 3–6. To compare the three adsorbents used, these models were applied to the adsorption data that were obtained by performing batch tests at an initial  $\text{Pb}^{2+}$  concentration of  $40 \text{ mg L}^{-1}$ .

$$q_t = q_e (1 - \exp(-k_1 t)) \quad (3)$$

$$q_t = \frac{q_e^2 k_2 \cdot t}{q_e k_2 \cdot t + 1} \quad (4)$$

$$q_t = \frac{1}{\beta} \ln(1 + \alpha \beta t) \quad (5)$$

$$q_t = K_p t^{1/2} + C \quad (6)$$

Both linear and nonlinear ( $q_t$  vs.  $t$ ) fitting was accomplished using the OriginPro 8.5 Software, and the estimated values (using the slope and intercept values in linear fitting) of the associated parameters in each model are listed in Table 2. In the above equations,  $q_t$  ( $\text{mg g}^{-1}$ ) is the uptake of  $\text{Pb}^{2+}$  by the adsorbent at any time  $t$ , while  $q_e$  (in Eqs 3 and 4) is measured experimentally and represents the equilibrium uptake capacity.  $k_1$  ( $\text{min}^{-1}$ ) and  $k_2$  ( $\text{mg g}^{-1} \text{min}^{-1}$ ) in Eqs (3) and (4) represent the rate constants of the pseudo-first-order (first-order) and pseudo-second-order (second-order) kinetic models, respectively. The initial adsorption rate constant

**Table 1. Comparison of the estimated adsorption capacities of various adsorbents for  $\text{Pb}^{2+}$  with investigated adsorbents in this study.**

Type of adsorbent	Maximum adsorption capacity, $\text{mg g}^{-1}$ (except where mentioned)	Reference
MgFe/LDH	116	This study
MgFe/LDH-Eb	119	This study
MgFe/LDH-Eb_EDTA	136	This study
$\text{Mg}_2\text{Al-LS-LDH}$	123	[51]
Kiwi branch Biochar/ZnFe-LDH	161.29	[35]
Rice husk ash/MgFe/LDH	682.2	[52]
Montmorillonite–illite type of clay	51.80	[53]
$\text{Fe}_3\text{O}_4/\text{GO}/\text{MgAl-LDH}$	173	[54]
ZnAl-LDH intercalated with EDTA	$871 \text{ umol g}^{-1}$	[55]
$\text{Mg}_2\text{Al-LDH}$	66.16	[56]
ZnAl-LDH/DTPA	$80 \text{ umol g}^{-1}$	[57]
Biochar/MgFe-LDH	476.25	[58]
EDTA-LDH/Biochar	146.84	[59]
$\text{Fe}_3\text{O}_4/\text{SiO}_2\text{-EDTA}$	114.94	[60]

<https://doi.org/10.1371/journal.pone.0265024.t001>

**Table 2.** Estimated values of the parameters using linearized and nonlinear kinetic models for 40 mg L<sup>-1</sup> Pb<sup>2+</sup> onto 0.3 g of adsorbent at pH = 6 ± 0.2.

Kinetic model	Parameter	MgFe/LDH		MgFe/LDH-Eb		MgFe/LDH-Eb_EDTA	
		Lin	N-lin	Lin	N-lin	Lin	N-lin
	$q_{e \text{ exp}} \text{ (mg g}^{-1}\text{)}$	97.32		99.95		117.04	
first-order	$q_{e \text{ cal}} \text{ (mg g}^{-1}\text{)}$	10.20	92.4	10.10	94.31	9.51	112.67
	$k_1 \text{ (min}^{-1}\text{)}$	0.010	0.52	0.006	0.54	0.011	0.47
	$R^2$	0.43	0.73	0.26	0.73	0.4	0.74
second-order	$q_{e \text{ cal}} \text{ (mg g}^{-1}\text{)}$	96.15	95.96	97.09	97.69	116.28	116.84
	$k_2 \text{ (g mg}^{-1} \text{ min}^{-1}\text{)}$	0.0116	0.0095	0.0321	0.0101	0.0119	0.0073
	$h \text{ (mg g}^{-1} \text{ min}^{-1}\text{)}$	107.53	87.85	303.03	96.10	161.29	99.66
	$R^2$	0.9999	0.95	0.9998	0.94	0.9999	0.94
Elovich	$\alpha \text{ (mg g}^{-1} \text{ min}^{-1}\text{)}$	3171.13	23876	6689.00	48664	2379.40	22503
	$\beta \text{ (g mg}^{-1}\text{)}$	7.60	0.13	7.30	0.14	9.45	0.11
	$R^2$	0.85	0.83	0.8	0.78	0.83	0.81
ID-WM	$K_{ip} \text{ (mg g}^{-1} \text{ min}^{1/2}\text{)}$	2.06	2.06	1.92	1.92	2.53	2.53
	$C \text{ (mg g}^{-1}\text{)}$	71.85	71.85	74.85	74.85	86.80	86.51
	$R^2$	0.52	0.45	0.46	0.41	0.5	0.45

<https://doi.org/10.1371/journal.pone.0265024.t002>

and activation energy are expressed by  $\alpha \text{ (mg g}^{-1} \text{ min}^{-1}\text{)}$  and  $\beta \text{ (g mg}^{-1}\text{)}$ , respectively, in the Elovich kinetic model (Eq 5). The rate constant and boundary-layer thickness of the intraparticle diffusion of Weber and Morris (ID-WM) kinetic model (Eq 6) are presented by  $K_{ip} \text{ (mg g}^{-1} \text{ min}^{1/2}\text{)}$  and  $C \text{ (mg g}^{-1}\text{)}$ , respectively.

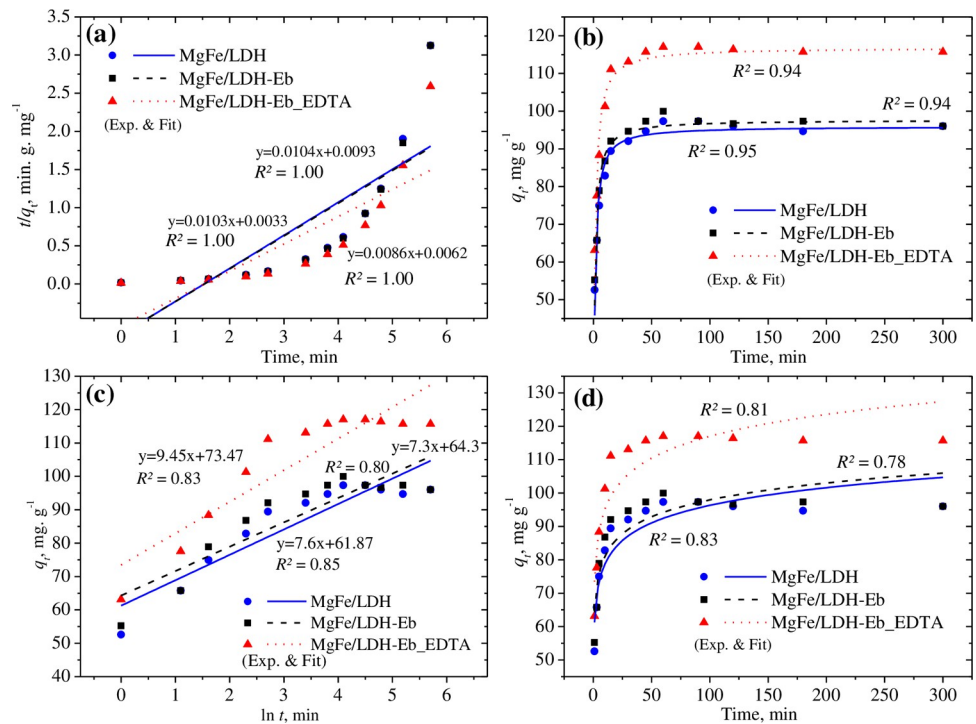


**Fig 5.** Linearized and nonlinear fitting of the second-order (a & b) and Elovich (c & d) kinetic models at 40 mg L<sup>-1</sup> Pb<sup>2+</sup>

<https://doi.org/10.1371/journal.pone.0265024.g005>

Linearized and nonlinear fittings of the second-order and Elovich kinetic models to the adsorption data of  $\text{Pb}^{2+}$  ( $40 \text{ mg L}^{-1}$ ) for all three adsorbents (0.3 g) are presented in Fig 5. A perfect linearized fitting of the second-order kinetic model (Fig 5A) is predicted based on the coefficient of determination ( $R^2$ ) value of 1.0 for all adsorbents, suggesting that chemisorption is the mechanism that controls adsorption [61–63]. The nonlinear fitting (Fig 5B) also generated high  $R^2$  values (0.95) for all adsorbents. Both the linearized and nonlinear fittings (Fig 5C and 5D) of the Elovich kinetic model produced nearly the same  $R^2$  values (close to 0.80) to fit the adsorption of  $\text{Pb}^{2+}$  on all three adsorbents.

As presented in Table 2, good  $R^2$  values (0.73) were recorded for the nonlinear fitting of the first-order kinetic model, and this result was further supported by a slight underestimation of the calculated maximum adsorption capacities in comparison to the experimental values (for example,  $113 \text{ mg g}^{-1}$  versus  $117 \text{ mg g}^{-1}$  for MgFe/LDH-Eb\_EDTA). Approximately the same  $k_1$  ( $0.5 \text{ min}^{-1}$ ) values for the nonlinear fitting of the first-order kinetic model were observed for all three adsorbents. A poor representation of the linearized first-order kinetic model can be predicted based on the calculated adsorption capacities and  $R^2$  values (Table 2) for the adsorption of  $\text{Pb}^{2+}$  onto the selected adsorbents. For the second-order kinetic model, the calculated adsorption capacities closely agreed with the experimental values for both the linearized and nonlinear fitting of the adsorption data using all three adsorbents, as presented in Table 2. The  $k_2$  and initial adsorption rate,  $h$ , ( $k_2 q_e^2$ ) in the nonlinear second-order kinetic model were estimated to be higher than the linearized fitting with the highest value of  $h$  ( $99.66 \text{ mg g}^{-1} \text{ min}^{-1}$ ) for MgFe/LDH-Eb\_EDTA in the nonlinear fitting.

The ID-WM kinetic model did not yield a reasonable fit to the adsorption data of  $\text{Pb}^{2+}$ , with  $R^2$  values in the range of 0.4–0.5 for both the linearized and nonlinear fittings, while both associated parameters,  $K_{ip}$  and  $C$ , were estimated to be nearly the same (Table 2) for both linearized and nonlinear fitting for all three adsorbents, and the highest  $R^2$  value was observed for MgFe/LDH-Eb\_EDTA ( $2.53 \text{ mg g}^{-1} \text{ min}^{1/2}$  and  $87 \text{ mg g}^{-1}$  for  $K_{ip}$  and  $C$ , respectively). The Elovich kinetic model was shown to be a better representation of the adsorption data than the first-order or ID-WM kinetic models based on the estimated  $R^2$  values in all three models. Both associated parameters,  $\alpha$  and  $\beta$ , in the Elovich kinetic model vary considerably for the linearized and nonlinear fitting, and MgFe/LDH-Eb\_EDTA had the lowest values except for  $\beta$  ( $9.45 \text{ g mg}^{-1}$  as shown in Table 2) in the linearized fitting.

### 3.4. Modeling of the experimental data using adsorption isotherms

To evaluate the adsorption performance, two- and three-parameter isotherm models were applied to the experimental batch test data. A description of the commonly applicable models is provided in Table 3, and both nonlinear and linearized fittings (wherever applicable) were used.

Fig 6 depicts the fitting of the linearized and nonlinear fittings of the selected two-parameter isotherm models, namely, the Langmuir and Freundlich models. Slope and intercept values were used in the linearized fitting to estimate the values of related parameters at  $60 \text{ mg L}^{-1} \text{ Pb}^{2+}$ , while isotherm models were fit using  $20\text{--}100 \text{ mg L}^{-1}$  of the studied metal ions with an adsorbent amount of 0.3 g. Suspensions were agitated for a contact time of 60 min by maintaining the solution pH at approximately 6.0. Slightly better fitting of the linearized model can be seen in comparison to the nonlinear fitting for both the Langmuir and Freundlich isotherm models for all three adsorbents, as predicted based on  $R^2$  values. The Langmuir model best presented the adsorption data with  $R^2$  values close to unity (1.0), which suggested monolayer adsorption had occurred, while the Freundlich model yielded  $R^2$  values of approximately 0.8.

**Table 3. Nonlinear expressions of the two- and three-parameter isotherm models and explanation of the parameters.**

Isotherm model	Mathematical expression	Parameters
Langmuir	$q_e = \frac{q_m K_L C_e}{(1 + K_L C_e)}$	$q_m$ , maximum sorption capacity, $\text{mg g}^{-1}$ $K_L$ , Langmuir constant, $\text{L mg}^{-1}$
Freundlich	$q_e = K_F C_e^{1/n}$	$K_F$ , Freundlich constant, $\text{L g}^{-1}$ $n$ , dimensionless constant
Dubinin–Radushkevich	$q_e = q_m \exp(-K_{DR} \epsilon^2)$ $\epsilon = RT \ln(1 + 1/C_e)$ $E = 1/\sqrt{2K_{DR}}$	$T$ , absolute temperature, Kelvin $R$ , universal gas constant, $8.314 \text{ J mol}^{-1} \cdot \text{K}^{-1}$ $E$ , mean free energy of adsorption, $\text{kJ mol}^{-1}$
Halsey	$q_e = \exp\left(\frac{\ln k_H - \ln C_e}{n_H}\right)$	$n_H$ and $k_H$ , Halsey constants
Temkin	$q_e = \frac{RT}{H_{ads}} \ln(K_T C_e)$	$A_T$ , equilibrium binding constant, $\text{L g}^{-1}$ $b_T$ , heat of adsorption, $\text{kJ mol}^{-1}$
Harkins–Jura	$q_e = \left(\frac{A_{HJ}}{B_{HJ} - \log C_e}\right)^{\frac{1}{2}}$	$A_{HJ}$ and $B_{HJ}$ , H–J constants
Jovanovic	$q_e = q_m [1 - \exp(-k_j C_e)]$	$k_j$ , Jovanovic constant
Elovich	$\frac{q_e}{q_m} = k_e C_e \exp\left(-\frac{q_e}{q_m}\right)$	$k_e$ , Elovich constant
Redlich–Peterson	$q_e = \frac{K_{RP} C_e}{1 + K_{RP} C_e^\beta}$	$\alpha$ , $\text{L mg}^{-1}$ $\beta$ (0–1), dimensionless $K_{RP}$ , R–P constant, $\text{L g}^{-1}$
Sips	$q_e = \frac{q_m K_S C_e^n}{1 + K_S C_e^n}$	$n$ , degree of heterogeneity, dimensionless $K_S$ , energy of adsorption, $\text{L g}^{-1}$

<https://doi.org/10.1371/journal.pone.0265024.t003>

As shown in Table 4, the predicted maximum adsorption capacities overestimated the experimental values for both models using all three adsorbents, although both values were closely matched for MgFe/LDH-Eb\_EDTA. A better affinity between the adsorbent surface

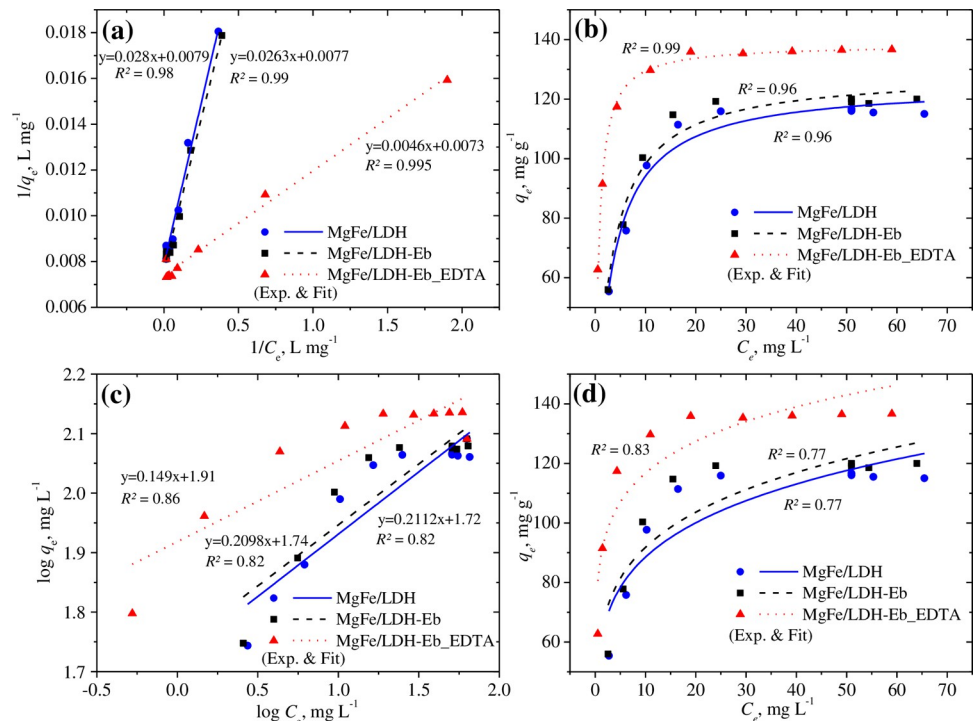


**Fig 6. Linearized and nonlinear fitting of the Langmuir (a & b) and Freundlich (c & d) isotherm models.**

<https://doi.org/10.1371/journal.pone.0265024.g006>

**Table 4. Values of parameters in the linearized (Lin) and nonlinear (N-Lin) fittings of isotherm models at 60 mg L<sup>-1</sup> Pb<sup>2+</sup> (solution pH = 6±0.2, contact time = 60 min, and adsorbent amount = 0.3 g).**

Isotherm	Parameter	MgFe/LDH		MgFe/LDH-Eb		MgFe/LDH-Eb_EDTA	
		Lin	N-Lin	Lin	N-Lin	Lin	N-Lin
	$q_{e\ exp}, \text{mg g}^{-1}$	115.89		119.23		135.89	
Langmuir	$q_m, \text{mg g}^{-1}$	126.58	125.11	129.87	128.73	136.99	138.34
	$K_L, \text{L mg}^{-1}$	0.28	0.30	0.29	0.32	1.59	1.45
	$R_L$	0.056	0.053	0.054	0.050	0.010	0.011
	$R^2$	0.98	0.96	0.99	0.96	0.995	0.99
Freundlich	$q_m, \text{mg g}^{-1}$	139.43	123.20	144.50	123.22	161.29	148.77
	$K_F, ((\text{mg/g})/(\text{L/mg})^{1/n})$	58.72	58.96	61.21	61.43	87.63	87.37
	$1/n$	0.211	0.180	0.210	0.170	0.149	0.130
	$R^2$	0.82	0.77	0.82	0.77	0.86	0.83
D-R	$q_m, \text{mg g}^{-1}$	111.71	113.38	115.40	117.12	130.63	132.03
	$K_{DR}, (\text{mol kJ}^{-1})^2$	1.0E-06	1.4E-06	1.0E-06	1.3E-06	1.0E-07	1.2E-07
	$E, \text{kJ mol}^{-1}$	0.71	0.59	0.71	0.61	2.24	2.02
	$R^2$	0.89	0.87	0.90	0.89	0.92	0.89
Halsey	$q_{e\ cal}, \text{mg g}^{-1}$	142.90	117.77	149.16	119.09	169.48	135.38
	$n_H$	-4.73	-5.67	-4.77	-5.76	-6.71	-7.99
	$K_H$	0.303	0.000	0.304	0.000	0.218	0.000
	$R^2$	0.82	0.77	0.82	0.77	0.86	0.83
Temkin	$K_T, \text{L mg}^{-1}$	13.09	13.10	14.40	14.40	281.28	281.29
	$H_{ads}, \text{kJ mol}^{-1}$	138.12	0.05	135.57	0.05	168.51	0.07
	$R^2$	0.86	0.83	0.85	0.83	0.9	0.89
H-J	$A_{HJ}, \text{mg g}^{-1}$	10000	516.4	80.12	119.15	12500	840.55
	$B_{HJ}$	3	3.9	-0.008	-0.21	2.5	4.64
	$R^2$	0.73	0.71	0.5	0.98	0.73	0.77
Jovanovic	$q_m, \text{mg g}^{-1}$	78.03	115.58	80.12	119.15	96.53	132.75
	$k_j, \text{L g}^{-1}$	-0.008	-0.2	-0.008	-0.21	-0.008	-0.93
	$R^2$	0.51	0.97	0.5	0.98	0.43	0.91
Elovich	$q_m, \text{mg g}^{-1}$	28.49		29.07		19.96	
	$k_e, \text{L g}^{-1}$	1.20		1.20		1.52	
	$R^2$	0.76		0.76		0.86	
R-P	$K_{RP}, \text{L g}^{-1}$		25.98		28.29		214.55
	$\alpha, \text{L mg}^{-1}$		0.13		0.13		1.61
	$\beta$		1.12		1.12		0.99
	$R^2$		0.98		0.99		1
Sips	$q_m, \text{mg g}^{-1}$		120.35		123.4		140.39
	$K_S, \text{L g}^{-1}$		0.21		0.21		1.39
	$n_S$		1.28		1.33		0.88
	$R^2$		0.96		0.97		1

<https://doi.org/10.1371/journal.pone.0265024.t004>

and the absorbed Pb<sup>2+</sup> was predicted for MgFe/LDH-Eb\_EDTA based on the  $K_L$  values (1.5 L mg<sup>-1</sup>, Table 4) in comparison to the other two adsorbents. The favorability of the Langmuir constant is further supported by the separation factor,  $R_L, [(1 + K_L C_0)^{-1}]$  which is in a suitable range of 0–1. The estimated values of  $K_F$  were highest for MgFe/LDH-Eb\_EDTA (Table 4), while the calculated values of the adsorption intensity ( $n > 1$ ) indicated the capability of the Freundlich model [64], as presented in Table 4.

The D–R isotherm also supported the adsorption data with  $R^2$  values close to 0.9 and with theoretical and experimental adsorption capacities that were close (Table 4), suggesting the adsorption system was physical since the estimated  $E$  values were below  $8 \text{ kJ mol}^{-1}$  for all adsorbents. The Temkin isotherm model provided a better representation of the adsorption data in comparison to the Halsey, H–J and Freundlich isotherm models, as reflected by the  $R^2$  values (0.83–0.90); thus, it is proposed that heterogeneous  $\text{Pb}^{2+}$  adsorption occurs with uniform dispersal of binding energies on the surface of adsorbents [65]. However, the nonlinear fitting of the Temkin isotherm yielded a very low adsorption heat, while the isotherm constant was the highest for MgFe/LDH-Eb\_EDTA ( $281 \text{ L mg}^{-1}$ , Table 4). In the case of the Jovanovic model, nonlinear fitting did improve the fitting to the adsorption data based on the  $R^2$  values (0.91–0.98, Table 4) in addition to generating a very close agreement for the calculated adsorption capacities and that of the experimental values for all adsorbents. A reasonable response was observed with the linearized Elovich model that explains the adsorption data based on the calculated  $R^2$  values; however, the theoretical adsorption capacities were greatly underestimated in comparison to the experimental values.

A very good response with both three-parameter models, Sips and R–P isotherms, was observed that explained the adsorption data, and the  $R^2$  values were close to unity (1.0); this reflected the homogeneous and heterogeneous adsorption of  $\text{Pb}^{2+}$  on the surface of adsorbents [66–69]. The calculated adsorption capacities were slightly overestimated in the case of the Sips isotherm model. The isotherm constant in the R–P model was much higher for MgFe/LDH-Eb\_EDTA than for the other adsorbents, and it had the highest adsorption energy ( $1.39 \text{ L g}^{-1}$ ) and lowest degree of heterogeneity (0.88, Table 4). Finally, based on the findings of isotherm models, surface adsorption seems to be less effective phenomenon as compared to the intraparticle diffusion through the internal surface of the studied adsorbents [70].

Considering the importance of the mechanistic study, results obtained from the characteristics of the loaded adsorbents are discussed to gain insights into the possible adsorption mechanisms. Heavy metal absorption and removal mechanisms using composites of various biochar and LDHs have been reported in many studies [71–73]. To comprehend the adsorption mechanism for MgFe/LDH and the composite adsorbents, samples before and after  $\text{Pb}^{2+}$  adsorption were analyzed. From all spectroscopic analysis and the results of kinetic and isothermal studies, it can be hypothesized that several mechanisms including the surface precipitation are involved in the adsorption of  $\text{Pb}^{2+}$  in this study. EDX analysis also revealed the ion exchange on the surface and in the interlayer of the synthesized adsorbent due to the change in the elemental contents of the loaded adsorbent. From the results of X-ray photoelectron spectroscopy (results not shown) slight shifting of binding energy towards the high energy side was seen after the composite adsorbent (MgFe/LDH-Eb) was loaded with  $\text{Pb}^{2+}$  and this suggests the involvement of hydroxide group in adsorption reaction due to the presence of the hydroxyl or deprotonated hydroxyl groups [74] on the surface of the loaded adsorbents. Moreover, stronger peaks in the loaded adsorbents (MgFe/LDH-Eb\_EDTA) with high binding energy suggest chelation with EDTA from the LDH interlayer.

## 4. Conclusions

In the current study, the LDH of MgFe and its composites with Eb and EDTA were developed and characterized, and their potential capacity to mitigate toxic  $\text{Pb}^{2+}$  from synthetic wastewater solutions was investigated. Clumping of flowers, such as MgFe/LDH ultrafine nano glitter microspheres that were entangled with each other, was seen in the SEM images of MgFe/LDH before and after  $\text{Pb}^{2+}$  adsorption, while porous and rough surfaces of biochar particles in addition to MgFe/LDH on the surface of biochar indicated that MgFe/LDH composites with Eb

were successfully formed. From the FTIR results, the appearance of new absorption bands after adsorption suggested that  $Pb^{2+}$  was successfully adsorbed onto the MgFe/LDH and composite adsorbents.

Batch tests yielded 60 min as an equilibrium contact time while a rapid removal rate of  $Pb^{2+}$  upon immediate contact with all adsorbents followed the gradual increase in adsorption capacity as well as removal efficiency. The maximum adsorption capacity and removal efficiency were  $63 \text{ mg g}^{-1}$  and 97%, respectively, for the composite adsorbent (MgFe/LDH-Eb\_EDTA) due to its high surface area proposing that techniques should be employed for increasing the surface area of adsorbents and that suitable retention time be provided for optimum performance of the adsorption system. Batch testing for optimizing the initial  $Pb^{2+}$  concentration suggested  $50 \text{ mg L}^{-1}$  as an optimum value since nearly insignificant increase in adsorption capacity was seen beyond this value while removal efficiency continued to decrease. Investigation on solution pH resulted a solution pH of 8.0 with best performance using the composite adsorbent signifying the wastewater solution to be neutralized before applying the adsorption system. An opposite trend of adsorption capacities and removal efficiency by changing the amount of adsorbents makes it difficult to select the optimum amount of the adsorbent and will vary depending upon the choice of the adsorption process. A maximum adsorption capacity of  $589 \text{ mg g}^{-1}$  with highest percentage removal (75%) at the lowest tested amount (0.05 g) for the composite adsorbent (MgFe/LDH-Eb\_EDTA) compared with other adsorbents signifies further the importance of selecting the adsorbent with high surface area.

A nearly perfect fitting of the second-order kinetic model based on the  $R^2$  value of 1.0 for all adsorbents suggested that chemisorption is the controlling mechanism of adsorption. Among the isotherm models, the Langmuir model best presented the adsorption data with  $R^2$  values that were close to unity (1.0); thus, the monolayer adsorption of  $Pb^{2+}$  was proposed. The D-R isotherm also supported the adsorption data with reasonable  $R^2$  values (approximately 0.9) and close theoretical and experimental adsorption capacities; thus, a physical adsorption system based on  $E$  values was proposed. The Temkin isotherm model provided a better representation of the adsorption data (with  $R^2$  values in the range 0.83–0.90) in comparison to that of the Halsey and H–J or even the Freundlich isotherm models, suggesting heterogeneous adsorption of  $Pb^{2+}$  occurred with uniform dispersal of binding energies on the surface of the adsorbent. Finally, an excellent representation of the adsorption data by both the Sips and R–P isotherms reflected homogeneous as well as heterogeneous adsorption of  $Pb^{2+}$  on the surface of adsorbents.

## Author Contributions

**Conceptualization:** M. T. Amin, A. A. Alazba.

**Data curation:** M. Shafiq.

**Formal analysis:** M. T. Amin, M. Shafiq.

**Funding acquisition:** A. A. Alazba.

**Investigation:** M. T. Amin, M. Shafiq.

**Methodology:** M. Shafiq.

**Project administration:** M. T. Amin, A. A. Alazba.

**Resources:** A. A. Alazba.

**Software:** M. Shafiq.

**Supervision:** M. T. Amin.

**Validation:** A. A. Alazba, M. Shafiq.

**Visualization:** M. Shafiq.

**Writing – original draft:** M. T. Amin, M. Shafiq.

**Writing – review & editing:** A. A. Alazba.

## References

1. Tchounwou PB, Yedjou CG, Patlolla AK, Sutton DJ. Heavy Metals Toxicity and the Environment. *EXS*. 2012; 101: 133–164. [https://doi.org/10.1007/978-3-7643-8340-4\\_6](https://doi.org/10.1007/978-3-7643-8340-4_6) PMID: 22945569
2. Li R, Wang JJ, Gaston LA, Zhou B, Li M, Xiao R, et al. An overview of carbothermal synthesis of metal-biochar composites for the removal of oxyanion contaminants from aqueous solution. *Carbon*. 2018; 129: 674–687. <https://doi.org/10.1016/j.carbon.2017.12.070>
3. Verma R, Vijayalakshmy K, Chaudhry V. Detrimental impacts of heavy metals on animal reproduction: A review. *J Entomol Zool Stud*. 2018; 6: 27–30.
4. Shafiq M, Alazba AA, Amin MT. Removal of Heavy Metals from Wastewater using Date Palm as a Biosorbent: A Comparative Review. *Sains Malaysiana*. 2018; 47: 35–49. <https://doi.org/10.17576/jsm-2018-4701-05>
5. Anwar J, Shafique U, Waheed-uz-Zaman, Salman M, Dar A, Anwar S. Removal of Pb(II) and Cd(II) from water by adsorption on peels of banana. *Bioresource Technology*. 2010; 101: 1752–1755. <https://doi.org/10.1016/j.biortech.2009.10.021> PMID: 19906528
6. Li J, Zheng L, Wang S-L, Wu Z, Wu W, Niazi NK, et al. Sorption mechanisms of lead on silicon-rich biochar in aqueous solution: Spectroscopic investigation. *Science of The Total Environment*. 2019; 672: 572–582. <https://doi.org/10.1016/j.scitotenv.2019.04.003> PMID: 30965268
7. Bouhamed F, Elouear Z, Bouzid J, Ouddane B. Batch sorption of Pb(II) ions from aqueous solutions using activated carbon prepared from date stones: equilibrium, kinetic, and thermodynamic studies. *Desalination and Water Treatment*. 2014; 52: 2261–2271. <https://doi.org/10.1080/19443994.2013.806222>
8. Villarreal JS, Gándara JR, Navarrete D, Bejarano ML, Landázuri AC. Lead (Pb<sup>2+</sup>) adsorption by means of pristine and prewashed residual *Moringa oleifera* Lam. seed husk biomass for water treatment applications. *International Journal of Sustainable Engineering*. 2020; 0: 1–13. <https://doi.org/10.1080/19397038.2020.1862350>
9. Daud MK, Nafees M, Ali S, Rizwan M, Bajwa RA, Shakoor MB, et al. Drinking Water Quality Status and Contamination in Pakistan. In: *BioMed Research International* [Internet]. Hindawi; 14 Aug 2017 [Accessed 14 Jan 2021] p. e7908183. <https://doi.org/10.1155/2017/7908183> PMID: 28884130
10. Salman M, Athar M, Farooq U, Rauf S, Habiba U. A new approach to modification of an agro-based raw material for Pb(II) adsorption. *Korean Journal of Chemical Engineering*. 2014; 31: 467–474. <https://doi.org/10.1007/s11814-013-0264-8>
11. Mireles S, Parsons J, Trad T, Cheng C-L, Kang J. Lead removal from aqueous solutions using biochars derived from corn stover, orange peel, and pistachio shell. *Int J Environ Sci Technol*. 2019; 16: 5817–5826. <https://doi.org/10.1007/s13762-018-02191-5>
12. Yin J, Deng C, Yu Z, Wang X, Xu G. Effective Removal of Lead Ions from Aqueous Solution Using Nano Illite/Smectite Clay: Isotherm, Kinetic, and Thermodynamic Modeling of Adsorption. *Water*. 2018; 10: 210. <https://doi.org/10.3390/w10020210>
13. Wang X, Yu S, Wu Y, Pang H, Yu S, Chen Z, et al. The synergistic elimination of uranium (VI) species from aqueous solution using bi-functional nanocomposite of carbon sphere and layered double hydroxide. *Chemical Engineering Journal*. 2018; 342: 321–330. <https://doi.org/10.1016/j.cej.2018.02.102>
14. Tran HN, Nguyen HC, Woo SH, Nguyen TV, Vigneswaran S, Hosseini-Bandegharai A, et al. Removal of various contaminants from water by renewable lignocellulose-derived biosorbents: a comprehensive and critical review. *Critical Reviews in Environmental Science and Technology*. 2019; 49: 2155–2219. <https://doi.org/10.1080/10643389.2019.1607442>
15. Amin MT, Alazba AA, Manzoor U. A Review of Removal of Pollutants from Water/Wastewater Using Different Types of Nanomaterials. *Advances in Materials Science and Engineering*. 2014; 2014: 1–24. <https://doi.org/10.1155/2014/825910>
16. Zhu K, Gao Y, Tan X, Chen C. Polyaniline-Modified Mg/Al Layered Double Hydroxide Composites and Their Application in Efficient Removal of Cr(VI). *ACS Sustainable Chem Eng*. 2016; 4: 4361–4369. <https://doi.org/10.1021/acssuschemeng.6b00922>

17. Adeleye AS. Engineered nanomaterials for water treatment and remediation: Costs, benefits, and applicability. *Chemical Engineering Journal*. 2016; 23.
18. Hefny R, Ibrahim MM, Morad D. Study of Adsorption Performance of Biochar for Heavy Metals Removal. *Journal of Engineering Research and Reports*. 2020; 19: 27–40. <https://doi.org/10.9734/jerr/2020/v19i417239>
19. Khan ZU, Khan WU, Ullah B, Ali W, Ahmad B, Ali W, et al. Graphene oxide/PVC composite papers functionalized with p-Phenylenediamine as high-performance sorbent for the removal of heavy metal ions. *Journal of Environmental Chemical Engineering*. 2021; 9: 105916. <https://doi.org/10.1016/j.jece.2021.105916>
20. Liu T, Lawluyv Y, Shi Y, Ighalo JO, He Y, Zhang Y, et al. Adsorption of cadmium and lead from aqueous solution using modified biochar: A review. *Journal of Environmental Chemical Engineering*. 2022; 10: 106502. <https://doi.org/10.1016/j.jece.2021.106502>
21. Syeda HI, Yap P-S. A review on three-dimensional cellulose-based aerogels for the removal of heavy metals from water. *Science of The Total Environment*. 2022; 807: 150606. <https://doi.org/10.1016/j.scitotenv.2021.150606> PMID: 34592292
22. Wang F, Guo Z. In situ growth of ZIF-8 on CoAl layered double hydroxide/carbon fiber composites for highly efficient absorptive removal of hexavalent chromium from aqueous solutions. *Applied Clay Science*. 2019; 175: 115–123. <https://doi.org/10.1016/j.clay.2019.04.013>
23. Sajid M, Basheer C. Layered double hydroxides: Emerging sorbent materials for analytical extractions. *TrAC Trends in Analytical Chemistry*. 2016; 75: 174–182. <https://doi.org/10.1016/j.trac.2015.06.010>
24. Yang F, Sun S, Chen X, Chang Y, Zha F, Lei Z. Mg–Al layered double hydroxides modified clay adsorbents for efficient removal of Pb<sup>2+</sup>, Cu<sup>2+</sup> and Ni<sup>2+</sup> from water. *Applied Clay Science*. 2016; 123: 134–140. <https://doi.org/10.1016/j.clay.2016.01.026>
25. Yanming S, Dongbin L, Shifeng L, Lihui F, Shuai C, Haque MA. Removal of lead from aqueous solution on glutamate intercalated layered double hydroxide. *Arabian Journal of Chemistry*. 2017; 10: S2295–S2301. <https://doi.org/10.1016/j.arabjc.2013.08.005>
26. Cheng X, Huang X, Wang X, Sun D. Influence of calcination on the adsorptive removal of phosphate by Zn–Al layered double hydroxides from excess sludge liquor. *Journal of Hazardous Materials*. 2010; 177: 516–523. <https://doi.org/10.1016/j.jhazmat.2009.12.063> PMID: 20060217
27. Ji H, Wu W, Li F, Yu X, Fu J, Jia L. Enhanced adsorption of bromate from aqueous solutions on ordered mesoporous Mg–Al layered double hydroxides (LDHs). *J Hazard Mater*. 2017; 334: 212–222. <https://doi.org/10.1016/j.jhazmat.2017.04.014> PMID: 28414999
28. Caporale AG, Pigna M, Dynes JJ, Cozzolino V, Zhu J, Violante A. Effect of inorganic and organic ligands on the sorption/desorption of arsenate on/from Al–Mg and Fe–Mg layered double hydroxides. *J Hazard Mater*. 2011; 198: 291–298. <https://doi.org/10.1016/j.jhazmat.2011.10.044> PMID: 22071258
29. Yanming S, Dongbin L, Shifeng L, Lihui F, Shuai C, Haque MA. Removal of lead from aqueous solution on glutamate intercalated layered double hydroxide. *Arabian Journal of Chemistry*. 2017; 10: S2295–S2301. <https://doi.org/10.1016/j.arabjc.2013.08.005>
30. Kubra KT, Salman MdS, Hasan MdN. Enhanced toxic dye removal from wastewater using biodegradable polymeric natural adsorbent. *Journal of Molecular Liquids*. 2021; 328: 115468. <https://doi.org/10.1016/j.molliq.2021.115468>
31. Amin MT, Alazba AA, Shafiq M. Successful Application of Eucalyptus Camdulensis Biochar in the Batch Adsorption of Crystal Violet and Methylene Blue Dyes from Aqueous Solution. *Sustainability*. 2021; 13: 3600. <https://doi.org/10.3390/su13073600>
32. Ma Y, Wang Y, Xie D, Gu Y, Zhu X, Zhang H, et al. Hierarchical MgFe-layered double hydroxide microsphere/graphene composite for simultaneous electrochemical determination of trace Pb(II) and Cd(II). *Chemical Engineering Journal*. 2018; 347: 953–962. <https://doi.org/10.1016/j.cej.2018.04.172>
33. Matusik J, Rybka K. Removal of Chromates and Sulphates by Mg/Fe LDH and Heterostructured LDH/Halloysite Materials: Efficiency, Selectivity, and Stability of Adsorbents in Single- and Multi-Element Systems. *Materials*. 2019; 12: 1373. <https://doi.org/10.3390/ma12091373> PMID: 31035314
34. Rezvani Z, Rad FA, Khodam F. Synthesis and characterization of Mg–Al-layered double hydroxides intercalated with cubane-1,4-dicarboxylate anions. *Dalton Trans*. 2014; 44: 988–996. <https://doi.org/10.1039/C4DT03152K> PMID: 25407836
35. Tan Y, Wan X, Zhou T, Wang L, Yin X, Ma A, et al. Novel Zn–Fe engineered kiwi branch biochar for the removal of Pb(II) from aqueous solution. *Journal of Hazardous Materials*. 2022; 424: 127349. <https://doi.org/10.1016/j.jhazmat.2021.127349> PMID: 34879556
36. Matusik J, Deng Y. Fumonisin B1 Interaction with Mg–Al and Mg–Fe Layered Double Hydroxides: Removal Efficiency and Mechanisms. *Materials*. 2020; 13: 4344. <https://doi.org/10.3390/ma13194344> PMID: 33003621

37. de Carvalho GC, de Moura M de FV, de Castro HGC, da Silva Júnior JH, da Silva HEB, dos Santos KM, et al. Influence of the atmosphere on the decomposition of vegetable oils: study of the profiles of FTIR spectra and evolution of gaseous products. *J Therm Anal Calorim*. 2020; 140: 2247–2258. <https://doi.org/10.1007/s10973-019-08960-9>
38. Benício LPF, Eulálio D, Guimarães L de M, Pinto FG, Costa LM da, et al. Layered Double Hydroxides as Hosting Matrices for Storage and Slow Release of Phosphate Analyzed by Stirred-Flow Method. *Materials Research*. 2018; 21. <https://doi.org/10.1590/1980-5373-mr-2017-1004>
39. Wang S-L, Wang P-C. In situ XRD and ATR-FTIR study on the molecular orientation of interlayer nitrate in Mg/Al-layered double hydroxides in water. *Colloids and Surfaces A: Physicochemical and Engineering Aspects*. 2007; 292: 131–138. <https://doi.org/10.1016/j.colsurfa.2006.06.014>
40. Nejati K, Akbari AR, Davari S, Asadpour-Zeynali K, Rezvani Z. Zn–Fe-layered double hydroxide intercalated with vanadate and molybdate anions for electrocatalytic water oxidation. *New J Chem*. 2018; 42: 2889–2895. <https://doi.org/10.1039/C7NJ04469K>
41. Wang Y, Yang L, Peng X, Jin Z. High catalytic activity over novel Mg–Fe/Ti layered double hydroxides (LDHs) for polycarbonate diols (PCDLs): synthesis, mechanism and application. *RSC Adv*. 2017; 7: 35181–35190. <https://doi.org/10.1039/C7RA05892F>
42. Karapinar N, Donat R. Adsorption behaviour of Cu<sup>2+</sup> and Cd<sup>2+</sup> onto natural bentonite. *Desalination*. 2009; 249: 123–129. <https://doi.org/10.1016/j.desal.2008.12.046>
43. Raji F, Pakizeh M. Study of Hg(II) species removal from aqueous solution using hybrid ZnCl<sub>2</sub>-MCM-41 adsorbent. *Applied Surface Science*. 2013; 282: 415–424. <https://doi.org/10.1016/j.apsusc.2013.05.145>
44. Gunay A. Application of nonlinear regression analysis for ammonium exchange by natural (Bigadiç) clinoptilolite. *Journal of Hazardous Materials*. 2007; 148: 708–713. <https://doi.org/10.1016/j.jhazmat.2007.03.041> PMID: 17445983
45. Manohar DM, Noeline BF, Anirudhan TS. Adsorption performance of Al-pillared bentonite clay for the removal of cobalt(II) from aqueous phase. *Applied Clay Science*. 2006; 31: 194–206. <https://doi.org/10.1016/j.clay.2005.08.008>
46. Zaghouane-Boudiaf H, Boutahala M, Arab L. Removal of methyl orange from aqueous solution by uncalcined and calcined MgNiAl layered double hydroxides (LDHs). *Chemical Engineering Journal*. 2012; 187: 142–149. <https://doi.org/10.1016/j.cej.2012.01.112>
47. Rajoriya RK, Prasad B, Mishra IM, Wasewar KL. Adsorption of Benzaldehyde on Granular Activated Carbon: Kinetics, Equilibrium, and Thermodynamic. *Chemical and Biochemical Engineering Quarterly*. 2007 [Accessed 22 Jul 2020].
48. Tang H, Zhou W, Zhang L. Adsorption isotherms and kinetics studies of malachite green on chitin hydrogels. *J Hazard Mater*. 2012;209–210: 218–225. <https://doi.org/10.1016/j.jhazmat.2012.01.010> PMID: 22284169
49. Chowdhury S, Mishra R, Saha P, Kushwaha P. Adsorption thermodynamics, kinetics and isosteric heat of adsorption of malachite green onto chemically modified rice husk. *Desalination*. 2011; 265: 159–168. <https://doi.org/10.1016/j.desal.2010.07.047>
50. Taty-Costodes VC, Fauduet H, Porte C, Delacroix A. Removal of Cd(II) and Pb(II) ions, from aqueous solutions, by adsorption onto sawdust of *Pinus sylvestris*. *Journal of Hazardous Materials*. 2003; 105: 121–142. <https://doi.org/10.1016/j.jhazmat.2003.07.009> PMID: 14623423
51. Huang G, Wang D, Ma S, Chen J, Jiang L, Wang P. A new, low-cost adsorbent: Preparation, characterization, and adsorption behavior of Pb(II) and Cu(II). *Journal of Colloid and Interface Science*. 2015; 445: 294–302. <https://doi.org/10.1016/j.jcis.2014.12.099> PMID: 25626135
52. Yu J, Zhu Z, Zhang H, Qiu Y, Yin D. Mg–Fe layered double hydroxide assembled on biochar derived from rice husk ash: facile synthesis and application in efficient removal of heavy metals. *Environ Sci Pollut Res*. 2018; 25: 24293–24304. <https://doi.org/10.1007/s11356-018-2500-6> PMID: 29948711
53. Oubagaranadin JUK, Murthy ZVP. Adsorption of Divalent Lead on a Montmorillonite–Illite Type of Clay. *Ind Eng Chem Res*. 2009; 48: 10627–10636. <https://doi.org/10.1021/ie9005047>
54. Zhang F, Song Y, Song S, Zhang R, Hou W. Synthesis of Magnetite–Graphene Oxide-Layered Double Hydroxide Composites and Applications for the Removal of Pb(II) and 2,4-Dichlorophenoxyacetic Acid from Aqueous Solutions. *ACS Appl Mater Interfaces*. 2015; 7: 7251–7263. <https://doi.org/10.1021/acsami.5b00433> PMID: 25791354
55. Pérez MR, Pavlovic I, Barriga C, Cornejo J, Hermosín MC, Ulbarri MA. Uptake of Cu<sup>2+</sup>, Cd<sup>2+</sup> and Pb<sup>2+</sup> on Zn–Al layered double hydroxide intercalated with edta. *Applied Clay Science*. 2006; 32: 245–251. <https://doi.org/10.1016/j.clay.2006.01.008>
56. Zhao D, Sheng G, Hu J, Chen C, Wang X. The adsorption of Pb(II) on Mg<sub>2</sub>Al layered double hydroxide. *Chemical Engineering Journal*. 2011; 171: 167–174. <https://doi.org/10.1016/j.cej.2011.03.082>

57. Pavlovic I, Pérez MR, Barriga C, Ulibarri MA. Adsorption of  $\text{Cu}^{2+}$ ,  $\text{Cd}^{2+}$  and  $\text{Pb}^{2+}$  ions by layered double hydroxides intercalated with the chelating agents diethylenetriaminepentaacetate and meso-2,3-dimercaptosuccinate. *Applied Clay Science*. 2009; 43: 125–129. <https://doi.org/10.1016/j.clay.2008.07.020>
58. Jia Y, Zhang Y, Fu J, Yuan L, Li Z, Liu C, Zhao D, Wang X. A novel magnetic biochar/MgFe-layered double hydroxides composite removing  $\text{Pb}^{2+}$  from aqueous solution: Isotherms, kinetics and thermodynamics. *Colloids and Surfaces A: Physicochemical and Engineering Aspects*. 2019; 567: 278–287. <https://doi.org/10.1016/j.colsurfa.2019.01.064>
59. Wang C, Wang H. Pb(II) sorption from aqueous solution by novel biochar loaded with nano-particles. *Chemosphere*. 2018; 192: 1–4. <https://doi.org/10.1016/j.chemosphere.2017.10.125> PMID: 29091791
60. Liu Y, Fu R, Sun Y, Zhou X, Baig SA, Xu X. Multifunctional nanocomposites  $\text{Fe}_3\text{O}_4@ \text{SiO}_2$ -EDTA for Pb (II) and Cu(II) removal from aqueous solutions. *Applied Surface Science*. 2016; 369: 267–276. <https://doi.org/10.1016/j.apsusc.2016.02.043>
61. Hameed BH, El-Khaiary MI. Batch removal of malachite green from aqueous solutions by adsorption on oil palm trunk fibre: Equilibrium isotherms and kinetic studies. *Journal of Hazardous Materials*. 2008; 154: 237–244. <https://doi.org/10.1016/j.jhazmat.2007.10.017> PMID: 18022316
62. Ayranci E, Duman O. Structural effects on the interactions of benzene and naphthalene sulfonates with activated carbon cloth during adsorption from aqueous solutions. *Chemical Engineering Journal*. 2010; 156: 70–76. <https://doi.org/10.1016/j.cej.2009.09.038>
63. Duman O, Özcan C, Gürkan Polat T, Tunç S. Carbon nanotube-based magnetic and non-magnetic adsorbents for the high-efficiency removal of diquat dibromide herbicide from water: OMWCNT, OMWCNT- $\text{Fe}_3\text{O}_4$  and OMWCNT- $\kappa$ -carrageenan- $\text{Fe}_3\text{O}_4$  nanocomposites. *Environmental Pollution*. 2019; 244: 723–732. <https://doi.org/10.1016/j.envpol.2018.10.071> PMID: 30384078
64. Malik PK. Use of activated carbons prepared from sawdust and rice-husk for adsorption of acid dyes: a case study of Acid Yellow 36. *Dyes and Pigments*. 2003; 56: 239–249. [https://doi.org/10.1016/S0143-7208\(02\)00159-6](https://doi.org/10.1016/S0143-7208(02)00159-6)
65. Kumar PS, Ramakrishnan K, Gayathri R. Removal of Nickel(II) from Aqueous Solutions by Ceralite IR 120 Cationic Exchange Resins. *Journal of Engineering Science and Technology*. 2010; 5: 232–243.
66. Gimbert F, Morin-Crini N, Renault F, Badot P-M, Crini G. Adsorption isotherm models for dye removal by cationized starch-based material in a single component system: Error analysis. *Journal of Hazardous Materials*. 2008; 157: 34–46. <https://doi.org/10.1016/j.jhazmat.2007.12.072> PMID: 18243538
67. Abtahi M, Mesdaghinia A, Saeedi R, Nazmara S. Biosorption of As(III) and As(V) from aqueous solutions by brown macroalga *Colpomenia sinuosa* biomass: kinetic and equilibrium studies. *Desalination and Water Treatment*. 2013; 51: 3224–3232. <https://doi.org/10.1080/19443994.2012.749034>
68. Naddafi K, Rastkari N, Nabizadeh R, Saeedi R, Gholami M, Sarkhosh M. Adsorption of 2,4,6-trichlorophenol from aqueous solutions by a surfactant-modified zeolitic tuff: batch and continuous studies. *Desalination and Water Treatment*. 2016; 57: 5789–5799. <https://doi.org/10.1080/19443994.2015.1005693>
69. Günay A, Arslankaya E, Tosun İ. Lead removal from aqueous solution by natural and pretreated clinoptilolite: Adsorption equilibrium and kinetics. *Journal of Hazardous Materials*. 2007; 146: 362–371. <https://doi.org/10.1016/j.jhazmat.2006.12.034> PMID: 17261347
70. Shahmirzadi MAA, Hosseini SS, Tan NR. Enhancing removal and recovery of magnesium from aqueous solutions by using modified zeolite and bentonite and process optimization. *Korean J Chem Eng*. 2016; 33: 3529–3540. <https://doi.org/10.1007/s11814-016-0218-z>
71. Wang S, Gao B, Li Y, Zimmerman AR, Cao X. Sorption of arsenic onto Ni/Fe layered double hydroxide (LDH)-biochar composites. *RSC Adv*. 2016; 6: 17792–17799. <https://doi.org/10.1039/C5RA17490B>
72. Vithanage M, Ashiq A, Ramanayaka S, Bhatnagar A. Implications of layered double hydroxides assembled biochar composite in adsorptive removal of contaminants: Current status and future perspectives. *Science of The Total Environment*. 2020; 737: 139718. <https://doi.org/10.1016/j.scitotenv.2020.139718> PMID: 32526569
73. Zhang L, Tang S, Jiang C, Jiang X, Guan Y. Simultaneous and Efficient Capture of Inorganic Nitrogen and Heavy Metals by Polyporous Layered Double Hydroxide and Biochar Composite for Agricultural Nonpoint Pollution Control. *ACS Appl Mater Interfaces*. 2018; 10: 43013–43030. <https://doi.org/10.1021/acsami.8b15049> PMID: 30431258
74. Gunawan P, Xu R. Direct Assembly of Anisotropic Layered Double Hydroxide (LDH) Nanocrystals on Spherical Template for Fabrication of Drug-LDH Hollow Nanospheres. *Chem Mater*. 2009; 21: 781–783. <https://doi.org/10.1021/cm803203x>